#### **Research Article**

Ayat Abdulhussien Molaa\* and Mohammed Abdulwhaab Abdulwahid

# Numerical and experimental study of the impact on aerodynamic characteristics of the NACA0012 airfoil

https://doi.org/10.1515/eng-2022-0506 received May 29, 2023; accepted July 31, 2023

Abstract: Using computational models and low-speed wind tunnel tests, the aerodynamic characteristics of the NACA 0012 airfoil with low Re numbers of  $(8 \times 10^4, 2 \times 10^5, 3 \times 10^5,$ and  $4 \times 10^5$ ) and angle of attack (AOA) ranging from  $0^\circ$ to 18° by two steps are examined. Using the same 3-D wind tunnel dimensions, numerical simulations were run. The software program ANSYS FLUENT was used to solve the mathematical model using the continuity equation, the Navier-Stokes equations, and the  $k-\omega$  shearstress transport turbulence model. Findings demonstrate that at all AOAs, there is a direct relationship between Reynolds numbers (Re), lift and drag coefficients, kinetic energy, and stall angle. The lift coefficient rises linearly as the AOA increases, peaking at 14°, the stall angle at higher Reynolds number. The lift coefficient was found to decline when the AOA was increased further, reaching its minimal value at an AOA of 18°. With a greater AOA, the airfoil's drag coefficient rises, creating turbulent flow. The eddies produced by the turbulence cause the flow to start separating from the airfoil surface as turbulence increases. As a result, the airfoil lift coefficient drops, and its drag coefficient rises at the same time, leading to poor performance. The validation of the numerical results through wind tunnel experiments provided confidence in the findings of the study.

**Keywords:** airfoil, drag coefficient, lift coefficient, NACA0012, angle of attack, low Reynolds number, turbulent flow

## Symbols and acronyms Symbols Description (SI Unit)

L	lift force (N)
D	drag force (N)
$\mathcal{C}_{ ext{L}}$	lift coefficient (–)
$C_{\mathrm{D}}$	drag coefficient (–)
$C_{ m p}$	pressure coefficient (–)
Re	Reynolds number (–)
$\boldsymbol{P}$	gage pressure (N/m²)
$C_{\rm L}/C_{\rm D}$	lift-to-drag ratio (Airfoil's performance
	coefficient)
С	chord length of an airfoil (m)
h	height of colored water in manometer ((m)
ū	velocity compounds in the direction (x) (m/s)
$\bar{v}$	velocity compounds in the direction (y ((m/s)
$\bar{\mathcal{W}}$	velocity compounds in the direction (z) (m/s)
$ar{F}$	external force acting on the fluid (N)
$\nabla$	del operator (–)
A	wing surface area (m²)
$u_{\rm s}$	free stream velocity (m/s)
$\overrightarrow{V}$	velocity vector (m/s)
$\Delta P$	pressure difference (N/m²)

#### **Greek symbols**

Crossbala	Decemination	CT	T T-0 3+1
Symbols	Description	ιoι	UIIIL

 $\rho_{\omega}$ ,  $\rho_a$  density of water and air (kg/m<sup>3</sup>)

 $\omega$  turbulence energy dissipation frequency (S<sup>-1</sup>)

 $\mu$  kinematic viscosity (kg/m s)

#### **Abbreviation**

Symbols Description (SI Unit) AOA,  $\alpha$  angle of attack (°)

NACA National Advisory Committee for

Aeronautics (–)

<sup>\*</sup> Corresponding author: Ayat Abdulhussien Molaa, Department of Thermal Mechanical Technical Engineering, Southern Technical University, Basrah, Iraq, e-mail: ayat.molaa@fgs.stu.edu.iq Mohammed Abdulwhaab Abdulwahid: Department of Thermal Mechanical Technical Engineering, Southern Technical University, Basrah, Iraq, e-mail: mohw2016@stu.edu.iq

SST shear stress transport (–)
CFD computational fluid dynamics (–)

#### 1 Introduction

Aerodynamics is the branch of aeronautical mechanics concerned with the study of the forces exerted by air and other gases affecting object motion. In military and civil fields, structures and equipment such as gliders, wind turbines, small aerial vehicles, and unmanned aerial vehicles are subject to low Reynolds (Re) numbers. In aerodynamics, an airfoil is a cross-sectional structure with a rounded leading edge and a curved surface tapering in the flow direction. The airfoil generates a lifting force at an angle perpendicular to the fluid flow and a drag force along the fluid flow direction. These dynamic properties are important in flight and power generation; hence, the airfoil gains vital scientific importance in fluid dynamics. Examples of airfoils are cross-sections of wings, fan blades, windmill blades, compressors, turbine blades in jet engines, water cylinders, aircraft vertical stabilizers, submarine fins, rotary wings, and certain fixed wings. Thin and streamlined airfoils, owing to their low lift and drag, are generally preferred in high-velocity aircraft, while thick airfoils with high lift and drag are often used in aircraft for carrying heavy weights. Airfoils can be divided into symmetrical and asymmetrical types in terms of their surface shape. Symmetrical airfoils have an upper surface and a lower surface of similar camber, whereas asymmetric airfoils have an upper surface that differs from the lower surface. Lift and drag have been widely studied to obtain accurate results for various engineering applications.

Sadikin et al. [1] numerically studied the dynamic properties of a symmetric NACA0012 airfoil at angles of attack (AOAs) ranging between -10° and 15° and Re of 3 × 10<sup>6</sup> using three perturbation models, namely, the Spalart– Allmaras, k-Realizable, and  $k-\omega$  shear-stress transport (SST) models. They concluded that the Realizable k-E turbulence model results in smooth airflow over the upper surface of the airfoil. This delayed flow separation contributes to an increase in the lift force. In contrast, the Spalart Allmaras and  $k-\omega$  SST turbulence models exhibit earlier flow separation due to the presence of a large separation bubble. Furthermore, the study found that increasing the AOA leads to a linear increase in the lift coefficient until the stall angle is reached. However, as the AOA continues to increase, the flow velocity decreases at the trailing edge of the upper surface of the airfoil. This decrease in flow velocity causes a reduction in lift force.

Shabur et al. [2] numerically examined the turbulent kinetic energy (TKE) distribution of a symmetrical NACA0012 airfoil with a chord length of 1 m using different AOAs and Re numbers and compared the specimen with another symmetrical but thicker NACA0018 airfoil. They found a linear relationship between TKE distribution and AOA, indicating that higher speeds result in increased disturbance. The NACA 0018 airfoil was observed to generate more turbulence compared to the NACA 0012 airfoil due to increased friction with air particles resulting from its thicker design. In aircraft applications, minimizing turbulence is crucial, leading to the recommendation of using the NACA 0012 winglet. Conversely, the NACA 0018 winglet is recommended for wind turbines, where turbulence is not a significant concern.

Martínez-Aranda et al. [3] experimented on a closed wind tunnel device to examine the effect of AOA and Re numbers  $(3.33 \times 10^4, 6.67 \times 10^4, 10^5, \text{ and } 1.33 \times 10^5)$  on the NACA0012 airfoil. As the Re numbers and AOA increased, the lift and drag coefficients increased until stall angles ranging between 12° and 14° were reached.

Singh [4] experimentally studied an open-circuit wind tunnel device with a symmetric NACA0012 airfoil composed of acrylic materials and 29 ports. The parameters included AOAs from –14° to +15° increased in 2° increments and air velocities of 6.94, 7.76, 8.5, and 9.82 m/s. The pressure outlets were connected to a pressure gauge that contained gasoline liquid whose density is less than that of water. As air was passed through the test chamber, the pressure on the airfoil surfaces varied, which led to different pressure gauge readings. The values were positive for the airfoil's lower surface but negative for the upper surface, and the generated lifting force increased linearly with increasing AOA until the stall angle of 12° was reached. Furthermore, the lift coefficient presented inverse and direct relationships with increasing Re values at negative and positive AOA values, respectively.

Koshy and Jacob [5] numerically studied a symmetric NACA0012 airfoil and compared its pressure and velocity distributions and flow characteristics to those of an asymmetric NACA 2424 airfoil by varying the AOAs at  $0^{\circ}$ ,  $6^{\circ}$ , and  $9^{\circ}$  with the Re number set to  $3\times10^{5}$ . The symmetric airfoil did not produce a lift at an AOA of  $0^{\circ}$  in contrast to the asymmetric airfoil. The difference can be explained by the specific designs of the symmetric and asymmetric airfoils (i.e., with and without a camber, respectively); nonetheless, the pressure and velocity distributions surrounding the airfoil surfaces were similar. The asymmetric airfoil, which produced more lifting force, was more efficient than the symmetric airfoil.

Raval et al. [6] numerically analyzed the flow characteristics of a symmetric NACA0012 airfoil with a chord length of 1 m and selected V = 51.45 m/s and AOAs ranging

between 10° and 22° for the k- $\epsilon$  turbulence model. They concluded that as the AOA increases, the lift coefficient shows a linear increase until it reaches its maximum value at an angle of approximately 18.4°, which is known as the stall angle. Beyond the stall angle, the lift coefficient rapidly decreases. Additionally, it was observed that as the AOA increases, the drag coefficient gradually increases until reaching the stall angle, after which it increases even more rapidly. This behavior is attributed to the adverse pressure gradient that continuously increases, ultimately leading to flow separation and a loss of lift.

Kumar [7] investigated the flow behavior of a symmetric NACA0012 airfoil with a chord length of 1 m using a  $k-\omega$  SST turbulence model set to an air velocity of 30 m/s and AOAs of 0°, 3°, 5°, 8°, 11°, 13°, 16°, and 18°. At an AOA of 0°, the pressure and velocity distribution around the airfoil were similar, resulting in no lift generation. As the AOA increased, both the lift and drag coefficients gradually increased until reaching the stall angle of 16°, which represents the optimal performance of the airfoil. However, further increasing the AOA caused the separation of the hydrodynamic boundary layer, creating a turbulence zone filled with vortices. This turbulence negatively impacted the performance of the airfoil, leading to decreased efficiency and potential suspension of its operation.

Mallela et al. [8] numerically analyzed the flow behavior of the NACA0012 airfoil in terms of lift, drag, and pressure and velocity distributions. The Mach number of the  $k-\omega$  SST turbulence model was 0.44, and the AOAs varied from -6° to 10° in 2° increments. It was observed that at negative AOAs, the pressure increases and the velocity decreases on the upper surface of the airfoil. Conversely, at positive AOAs, the pressure decreases and the velocity increases on the upper surface of the airfoil. It was concluded that the lift coefficient initially has negative values for negative AOAs, but these values increase and become positive as the AOA increases. The lift coefficient reaches its optimal value at an angle of 10°. On the other hand, the drag coefficient decreases at negative AOAs but gradually increases as the AOA becomes positive.

Paper and Muramatsu [9] experimentally studied the effect of AOAs varying from 0° to 15° on the pressure distribution and bubble separation behavior of the NACA0012 airfoil at low Re numbers ranging from  $1 \times 10^4$  to  $5 \times 10^4$ . For the closed wind tunnel device, the airfoil had a chord length of 75 mm, and its 70 pressure ports were distributed on the two surfaces. Based on the pressure distributions, the study concluded that before reaching the stall angle, a short separation bubble appeared at Re numbers of  $3 \times 10^4$ and  $5 \times 10^4$ . However, after the stall angle, there was a

transition from a short bubble to a long bubble at Re numbers of  $3 \times 10^4$  and  $5 \times 10^4$ . At Re =  $1 \times 10^4$ , it was observed that the separation bubble moved toward the leading edge with an increasing AOA, indicating the formation of a long bubble on the airfoil surface. In addition, it was concluded that the lift coefficient curve exhibits different behaviors within specific AOA ranges. From 0° to 2°, the lift coefficient curve is zero. From 3° to 4°, it increases rapidly. From 5° to 9°, it increases slightly. From 9° to 12°, it becomes negative. Finally, from 12° to 15°, it remains constant.

Kabir et al. [10] numerically studied the aerodynamic properties of a symmetric NACA0012 airfoil. The  $k-\omega$  and turbulence models used parameters such as Mach number and AOAs ranging between -15° and 15° in 5° increments. The increasing AOA caused a pressure difference above and below the airfoil's surface, and a vortex was observed at the trailing edge of the airfoil. Additionally, the drag coefficient decreased before the AOA reached 0°, but it gradually increased with increasing AOAs.

Shahariar [11] numerically studied and compared the flow behaviors of two symmetric airfoils, namely, NACA0012 and asymmetric NACA4412, with the same chord lengths of 1 m. In the  $k-\varepsilon$  turbulence model, the AOAs were varied from  $0^{\circ}$  to  $25^{\circ}$  in  $5^{\circ}$  increments at Re =  $3 \times 10^{5}$ . A linear relationship was observed between the lift and drag coefficients and the AOAs until the stall angle of 16° was reached. Then, the lift coefficient decreased, while the drag coefficient increased rapidly for both airfoils. The findings were more prominent for the upper and lower surfaces of the NACA4412 airfoil.

Sahoo and Maity [12] numerically analyzed three airfoils with the same chord lengths of 1 m: one of them was symmetrical (NACA0012), whereas the other two were asymmetrical (NACA4412 and S809). Six turbulence models were used, the AOAs varied between 0° and 20°, and the air velocity was set to 51 m/s. They concluded that the  $(k-\omega SST)$ turbulence model provides results that closely match experimental data and is particularly effective in capturing shear transport. Additionally, it was observed that the NACA 4412 airfoil, with its thin profile and camber height, generates a higher lift coefficient compared to the NACA 0012 and S809 airfoils.

Jha et al. [13] numerically investigated a symmetric NACA0012 airfoil at Re numbers of 2.21  $\times$  10<sup>5</sup> and 2.81  $\times$ 10<sup>5</sup> and AOAs of 0°, 5°, 10°, and 20° and validated the findings by comparing them with the experimental results. An SAS turbulence model on a simulated adaptive scale was used for the numerical study, while an open-circuit subsonic wind tunnel apparatus was used for the experimental study. The relationship between the lift coefficient and AOAs was linear until the peak of 13° was reached; this finding was consistent with the experimental results. Moreover, the lift coefficient decreased, while the drag coefficient increased with increasing Re numbers.

Yousefi and Razeghi [14] examined the varying effects of Re numbers and AOAs on the turbulent laminar transitions of three symmetric airfoils, namely, NACA0012, NACA0015, and NACA0018. They found that the location of laminar–turbulent transition on an airfoil is significantly influenced by the Reynolds number. As the Reynolds number decreases, the transition point moves closer to the downstream region of the airfoil. For the NACA 0012, 0015, and 0018 airfoils, the lower critical Reynolds numbers for flow were determined to be  $1 \times 10^5$ ,  $5 \times 10^4$ , and  $3.5 \times 10^4$ , respectively. Furthermore, it was found that the transition location varies with the AOA. As the AOA increases, the transition point shifts toward the leading edge of the airfoil.

Eftekhari and Al-Obaidi [15] studied the effect of AOAs (0° and 90°) on the aerodynamic properties of an airfoil at low Re numbers (1 × 10<sup>5</sup>, 2 × 10<sup>5</sup>, and × 10<sup>5</sup>). The findings were validated by comparing them with the results of an experimental study involving a wind tunnel device. The flow separation started upon reaching 5°; at this time, vortices were formed and the lift coefficient decreased. Furthermore, the drag coefficient gradually increased up to an angle of 74° and decreased slightly between 74° and 82°, after which it settled at 90°. The rapidly increasing drag coefficient resulted in a decreasing lift coefficient, which agreed well with the experimental results.

The aerodynamics of airfoil surfaces, particularly the NACA0012 airfoil, have been the subject of numerous earlier investigations and studies. However, other important factors have not been fully examined, including pressure distribution, low Re numbers, and AOA. Many studies concentrated on examining the effects of certain factors, including low Reynolds number or AOA. These previously unconsidered factors are now given importance in the current study, which covers a wider range of low Re numbers  $(8 \times 10^4, 2 \times 10^5, 3 \times 10^5)$  $10^5$ , and  $4 \times 10^5$ ) and various AOAs (0°–18° with 2° increments). The goal of this study is to examine how they affect the pressure and velocity distribution on the airfoil as well as the lift and drag coefficients. This study offers designers a more complete understanding of airfoil aerodynamics by combining data on lift and drag coefficients as well as pressure distribution. It promotes the design of high-performance, more effective airfoil shapes.

#### 2 Experimental study

Laboratory wind tunnels are frequently used for experimental investigations on aerodynamic qualities. Laboratory

wind tunnels offer an efficient and practical alternative to airborne laboratory wind tunnel equipment that is limited in accessibility while producing reliable data. There are two different types of wind tunnels that are described: closed wind tunnels, where air circulates inside the tunnel, and open-circuit wind tunnels, where air enters and leaves the tunnel from the atmosphere.

The experimental study focuses on investigating the low-speed aerodynamic properties of a NACA0012 airfoil at Re numbers of  $8\times 10^4$  and  $2\times 10^5$  using an open-circuit wind tunnel apparatus. The experiment was carried out in the Al-Furat Al-Awsat Technical University/Engineering Technical College's Fluid Mechanics Laboratory in Najaf. The main objective of the experimental research is to validate the numerical results. Wind tunnel parts are depicted in Figure 1.

#### 2.1 Stages of the experimental work

As shown in Figure 1, a separate control and instrumentation unit control the wind tunnel apparatus. The dynamic conical form of the structure causes the air to flow and accelerate linearly as it enters via the effuser. The air then goes to the work section, a square area with dimensions of 305, 305, 600 mm and was constructed of acrylic material. The sides of the work section are moveable, while the upper and lower portions are fixed. Pitot tubes attached to two manometers, which are used to detect static pressure, can be inserted through two holes in the upper portion. A special holder for installing the airfoil is located on one side, and a special holder for connecting the other portion of the airfoil to a device that measures angles so that the aileron angle may be adjusted is located on the other side. The air then travels via a grid to the axial fan (the grid safeguards the fan from harm), then it travels through the silencer unit before reaching the atmosphere.

The pressure display unit, which has 32 pressure ports, displays the pressure results for each point of the airfoil. A single-component lift and drag balance unit determines the lift and drag forces for each angle. Bernoulli's equation (1) is used to compute the changing air velocity, which is tracked by a separate control and instrumentation unit, while equation (2) is used to determine the Re numbers [6]:

$$u_{\rm s} = \sqrt{\frac{2gh\rho_{\rm \omega}}{\rho_{\rm a}}},\tag{1}$$

$$Re = \frac{\rho_a u_s C}{\mu_a}.$$
 (2)

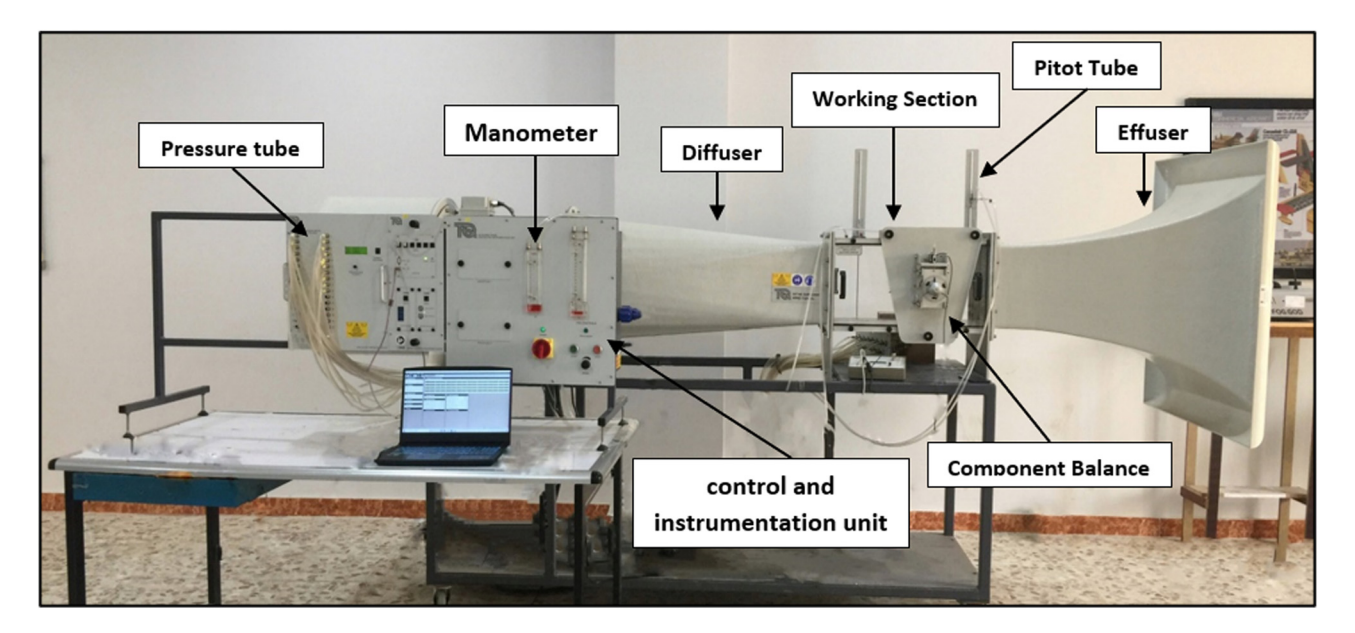


Figure 1: Subsonic wind tunnel AF100.

A symmetrical NACA0012 airfoil was used as the study's model. The airfoil was 300 mm wide and 150 mm in chord. Twenty pressure tappings were installed along its chord as part of its equipment. The tiny diameter tubes that protruded from the airfoil's end were attached to these tappings. The tubes might connect to a bigger diameter pipe by being further attached to labeled flexible pipes using adaptors. By adjusting the opposite end of the airfoil, the AOA of the airfoil may be changed.

#### 3 Numerical study

The ANSYS FLUENT 2021 R2 software package was used for airfoil engineering and construction. Flux simulations were performed at Re =  $8 \times 10^4$ ,  $2 \times 10^5$ ,  $3 \times 10^5$ , and  $4 \times 10^5$ . The flow was set in static and incompressible states, and the airfoil was in 3D. The turbulent viscosity coefficient was calculated using the  $k-\omega$  SST turbulence model that consisted of two equations, namely, the conservation equation and two transport equations. The two input variables were the TKE (k) for determining the energy in turbulence and the specific turbulent dissipation rate ( $\omega$ ) for determining the dissipation rate per unit of perturbed kinetic energy.

 $\omega$  is also referred to as the turbulence measure, which is suitable for modeling thick boundary layers for flows with low Re numbers. The  $k-\omega$  SST turbulence model is one of the most widely used models for determining the effect of turbulent flow conditions, and it is best used for near-wall processing. The  $k-\omega$  SST turbulence model can also predict excessive and early separation, has a better

convergence rate and behavior than other turbulence models for opposite pressure gradients, and requires low-memory computation.

For the four digits of the NACA0012 non-cambered airfoil, 00 indicates the non-cambered symmetric biplane airfoil and 12 indicates the airfoil thickness of 12% chord length.

#### 3.1 Mathematical model

The first stage of the numerical study was the mathematical model, which included integral equations and boundary conditions. The 3D continuity equation and momentum equations are given by [16]:

Continuity equation: 
$$\nabla \cdot \vec{V} = 0$$
. (3)

Momentum equations:

$$x\text{-direction }\rho\left[\bar{v}\frac{\partial\bar{u}}{\partial x} + \bar{v}\frac{\partial\bar{u}}{\partial y} + \bar{w}\frac{\partial\bar{u}}{\partial z}\right] = -\frac{\partial\bar{P}}{\partial x} + \mu\nabla^2\bar{u}$$

$$+ \bar{F}(\text{turb}, x),$$
(4)

y-direction 
$$\rho \left[ \overline{u} \frac{\partial \overline{v}}{\partial x} + \overline{v} \frac{\partial \overline{v}}{\partial y} + \overline{w} \frac{\partial \overline{v}}{\partial \overline{z}} \right]$$
  
=  $-\frac{\partial \overline{P}}{\partial y} + \mu \nabla^2 \overline{v} + \overline{F}(\text{turb}, y),$  (5)

z-direction 
$$\rho \left[ \bar{u} \frac{\partial \bar{w}}{\partial x} + \bar{v} \frac{\partial \bar{w}}{\partial y} + \bar{w} \frac{\partial \bar{w}}{\partial z} \right]$$
  
=  $-\frac{\partial \bar{P}}{\partial z} + \mu \nabla^2 \bar{w} + \bar{F}(\text{turb}, z),$  (6)

In order to compare the results with the experimental test inside the wind tunnel, the same dimensions of the test tunnel and the available wing model in the laboratory were used. Table 1 shows the input parameters of the airfoil. For the modeling, the symmetric airfoil data of NACA0012 were imported from the website [17] into the ANSYS FLUENT platform. Figure 2 shows the boundary conditions. The boundary conditions are defined as follows:

- Inlet section: the velocity of the inflow is set at 8.08, 20.21, 30.31, and 40.42 m/s.
- Outlet section is the outlet pressure (P = 0).
- The no slip wall condition is selected.

#### 3.2 Mesh configuration

The mesh was built using the ANSYS FLUENT platform to simulate the NACA0012 airfoil. Figure 3 shows the construction and intensification of the mesh around the airfoil, allowing for the visualization of the flow separation while obtaining the most accurate results (Table 2).

Table 1: Input parameters for the NACA0012 airfoil

Chord	150 mm
Span	300 mm
Area	$0.045  \text{m}^2$

#### 3.3 Setting up FLUENT

The geometry and mesh data were imported into the ANSYS FLUENT platform for initialization and solver operations. Increasing the kinetic energy would affect the flow of low-viscosity fluids and form vortices of various sizes and thus can be regarded as unstable. Table 3 shows the simulation parameters. Here, "Coupled" was used as a method for pressure\_velocity coupling, "Least squares cell based" was used for the spatial discretization section, and "First-order Upwind" and "Second-order upwind" were used to solve the momentum and obtain acceptable and good solutions for the turbulent dissipation rate and TKE. The program was initialized before calculation, and then, the calculation was run.

#### 4 Mesh independence

High-accuracy results of the numerical solution were obtained using several mesh elements, taking into account computer memory and time limitations. In general, large mesh elements require more computer memory and time. Here, the mesh size and its effect on the numerical simulation were verified by testing five mesh element sizes (1,034,566, 1,343,782, 2,246,431, 2,676,481, and 3,476,882) and subsequently obtaining the most accurate results within reasonable time and suitable computer memory. The mesh independence test was performed at Re =  $8 \times 10^4$ , and the ratio ( $C_L/C_D$ ) with AOAs ranging between  $0^\circ$  and  $18^\circ$  was analyzed for the symmetric NACA0012 airfoil. The test findings presented 2,246,431, 2,676,481, and 3,476,882 as the

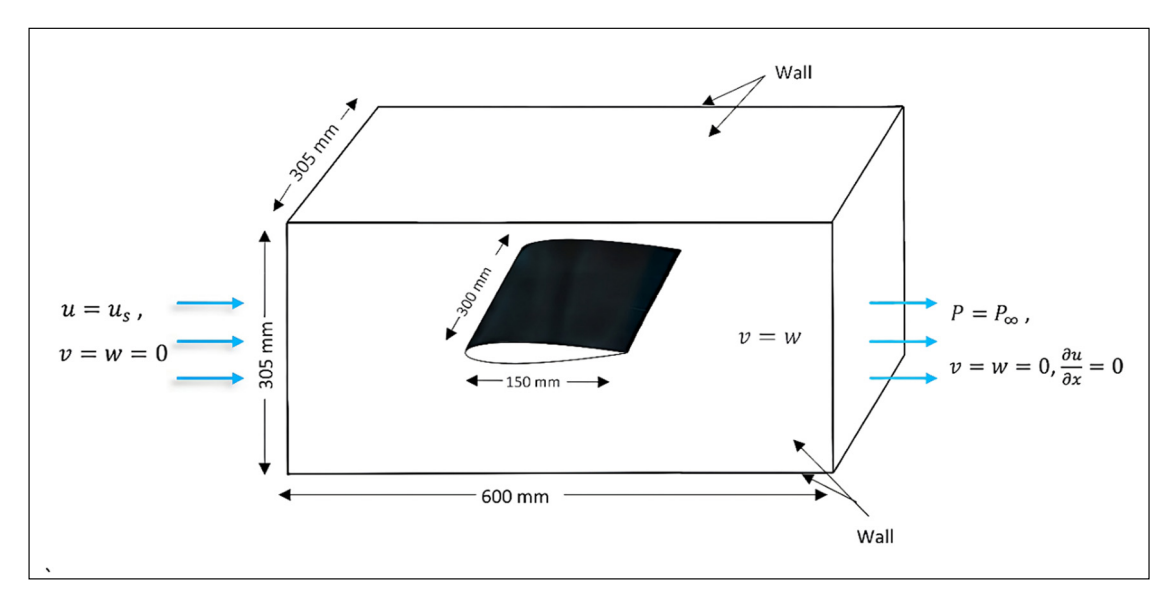


Figure 2: Schematic diagram of the NACA0012 airfoil.

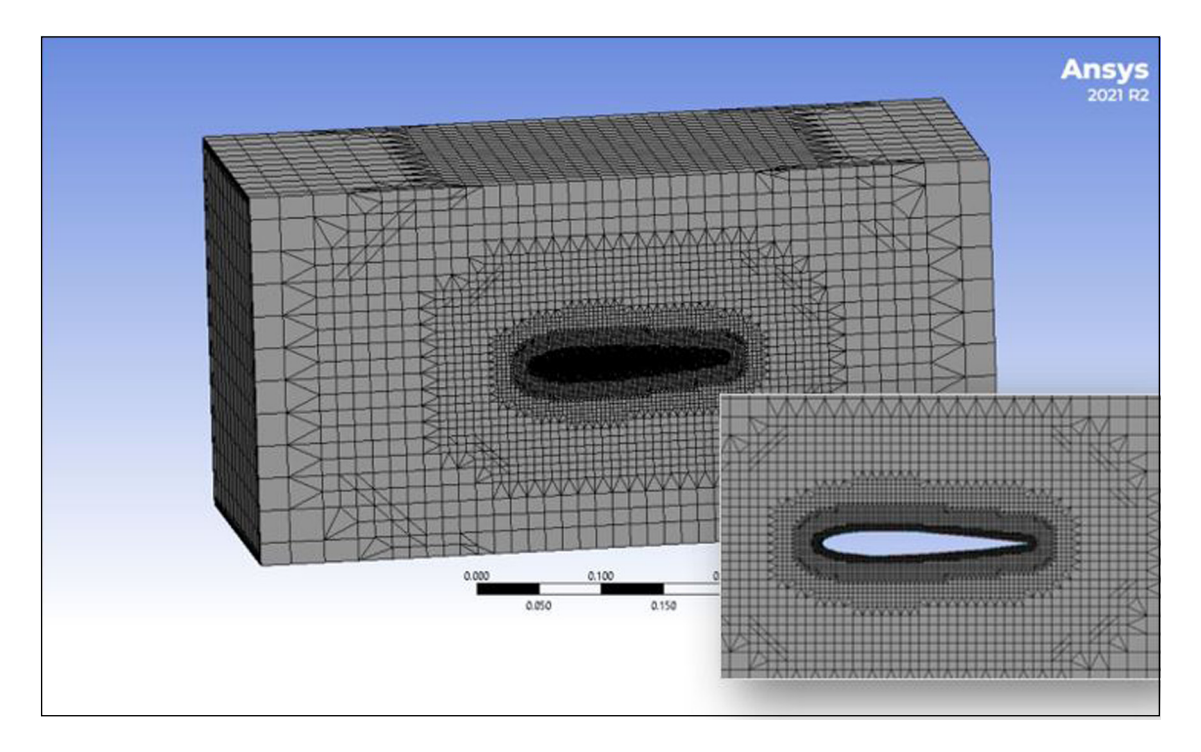


Figure 3: Mesh for the NACA0012 airfoil and the airfoil domain.

Table 2: Mesh input parameters

No. of nodes	2,802,362
No. of mesh elements	2,675,103
Maximum aspect ratio	2.798
Minimum orthogonal quality	0.9533

three mesh element sizes. These sizes attained almost the same results, but with varying times and computer memory requirements. Finally, 2,676,481 for the mesh element size with the most accurate results and reasonable time and computer memory requirements was selected (Figure 4).

#### 5 Validation

The numerical results of the published research of Patel and Thakor [7] were examined on the ANSYS FLUENT

Table 3: Input data for FLUENT simulation

Viscous model	k-ω SST (two equations)
Operating temperature	293 K
Operating pressure	0.0 Pa
Density of fluid	1.204 kg/m <sup>3</sup>
Kinematic viscosity	1.825 kg/m s
AOAs	0°-18° steps by 2°

platform with the objective of ensuring the accuracy and reliability of the current research's results. In particular, the test was conducted by comparing the results of the lift and drag coefficients on the symmetric NACA0012 airfoil with a chord length of 1 m at different AOAs (0°, 3°, 5°, 8°, 11°, 13°, 16°, and 18°) and  $u_{\rm s}=30$  m/s. The trends in Figures 5 and 6 indicate the high likelihood of adopting the code for the study. The results of the current research are highly compatible with those obtained by the previous work [7], indicating high reliability.

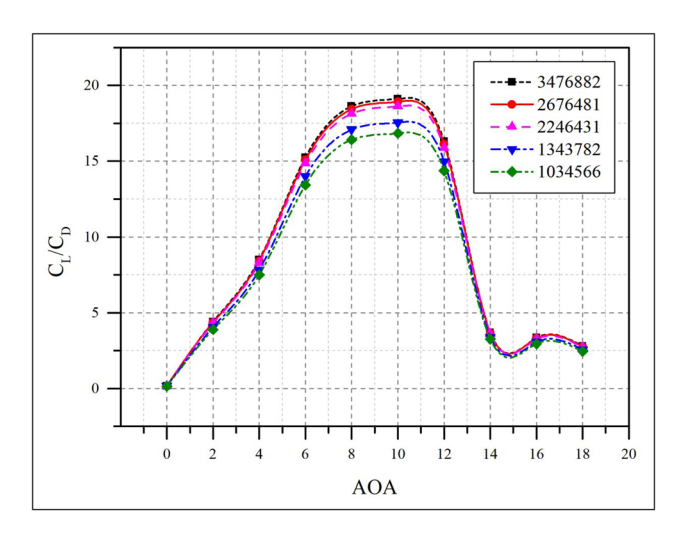
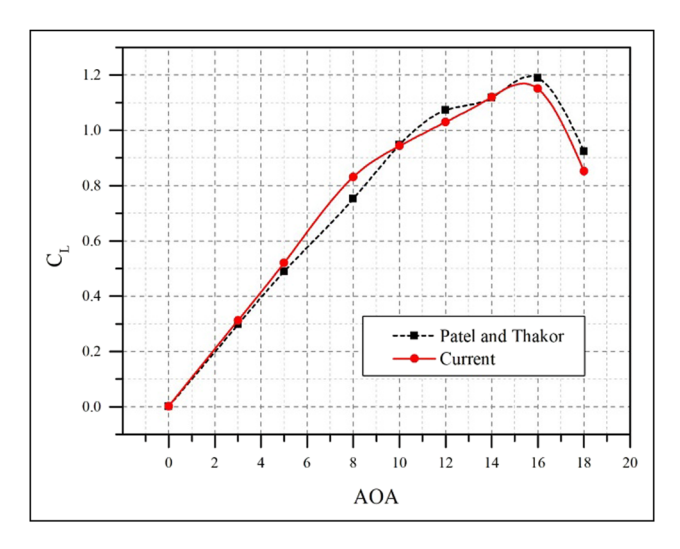
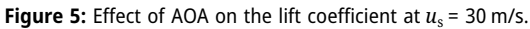
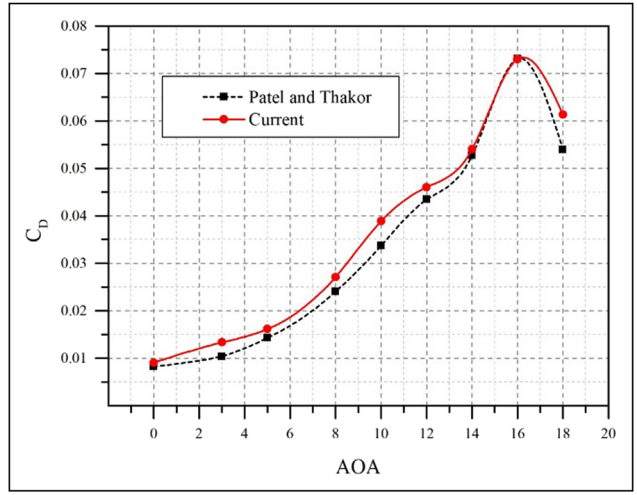


Figure 4: Mesh independence.







**Figure 6:** Effect of AOA on the drag coefficient at  $u_s = 30$  m/s.

#### 6 Results and discussion

### 6.1 Effects of pressure, velocity, and TKE on the NACA0012 airfoil

The TKE behavior, pressure, and velocity distributions on the surfaces of the NACA0012 airfoil are affected by the changes in both AOAs and Re numbers. Figures 7-9 show the TKE behavior, pressure, and velocity distributions surrounding the upper and lower surfaces of the airfoil. At an AOA of 0°, the pressure and velocity are distributed similarly around the airfoil. When increasing AOA, the pressure increases more prominently at the lower surface than at the upper surface; this trend is inconsistent with the changing velocity distribution, which more prominently increases at the upper surface than at the lower surface. The finding is in line with Bernoulli's principle, which states that fluid pressure rises as velocity decreases, and vice versa. The TKE starts to increase from the trailing edge until the stall angle is reached. However, further increasing the AOA causes the flow to separate and move toward the front edge of the airfoil, which can be explained by the changing pressure distribution. As the pressure increases at the upper surface and decreases at the lower surface, the velocity distribution changes (i.e., it increases at the lower surface and decreases at the upper surface), and the TKE increases along the upper surface of the airfoil. This situation results in the formation of vortices and the occurrence of chaos and turbulence, eventually causing airfoil failure; this phenomenon is called stalling. The pressure and velocity distributions and the TKE values are directly proportional to the increasing Re numbers.

#### 6.2 Effect of the AOA on $C_L$ and $C_D$

The variations in AOA affect the rise and fall of the airfoil as well as its stopping state. Tables 4 and 5 show the numerical and experimental results for the Cl and Cd for AOAs ranging from 0° to 18°, with a 2° increase at various Re numbers. The NACA 0012 airfoil is surrounded on both of its surfaces by the same pressure and velocity distributions due to its non-cambered form, so the pressure difference is equal to zero. According to equation (7), which represents the calculation formula for the lift force with pressure differences, the airfoil does not produce lift at an AOA of 0°. With increasing AOA, the lift coefficient increases and is directly proportional to the AOA, as illustrated in Figure 10, while the drag coefficient gradually increases until the stall angle is reached (Figure 11). This finding can be explained by the difference in pressure and velocity distributions between the lower and upper surfaces. However, further increasing the AOA causes a sudden and rapid decrease of the lift coefficient, and the drag coefficient exhibits dramatic behavior. This finding can be explained by the formation of vortices that extend from the trailing edge to the leading edge of the airfoil, further increasing the turbulence intensity and causing complete flow separation. Then, the lift coefficient is decreased at high AOAs, whereas the drag coefficient is increased, finally causing airfoil failure:

$$L = A \times \Delta P. \tag{7}$$

The solution was validated by comparing the numerical results with the experimental results. Figures 12 and 13 show the behavior of  $C_{\rm L}$  and  $C_{\rm D}$  with AOA at Re = 8 × 10<sup>4</sup>. The  $C_{\rm L}$  and  $C_{\rm D}$  curves for AOAs of 0°–8° agree well between

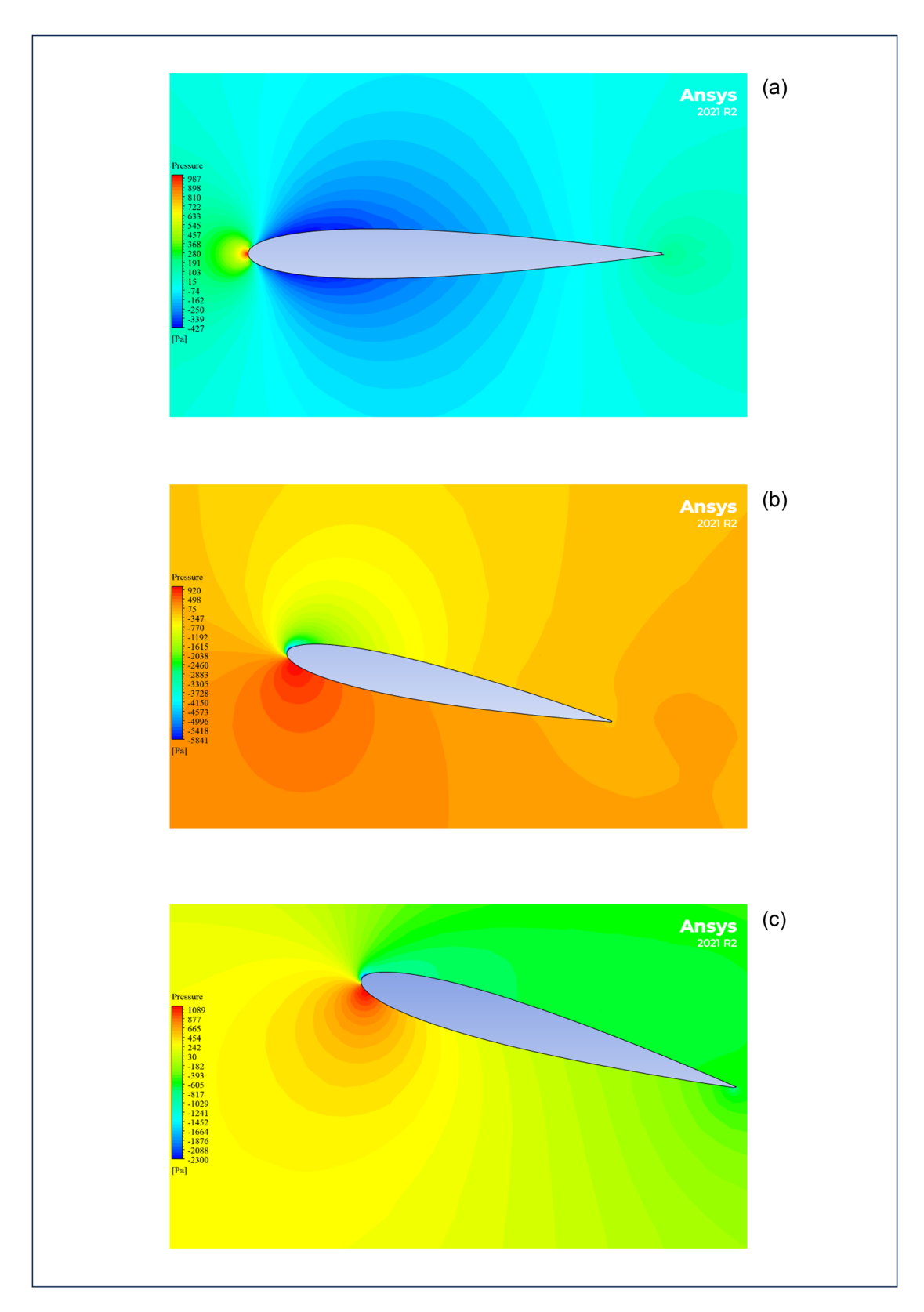


**Figure 7:** Pressure profiles of airfoil NACA0012 that  $Re = 4 \times 10^5$  and at AOA: (a) = 0°, (b) = 14°, and (c) = 18°.

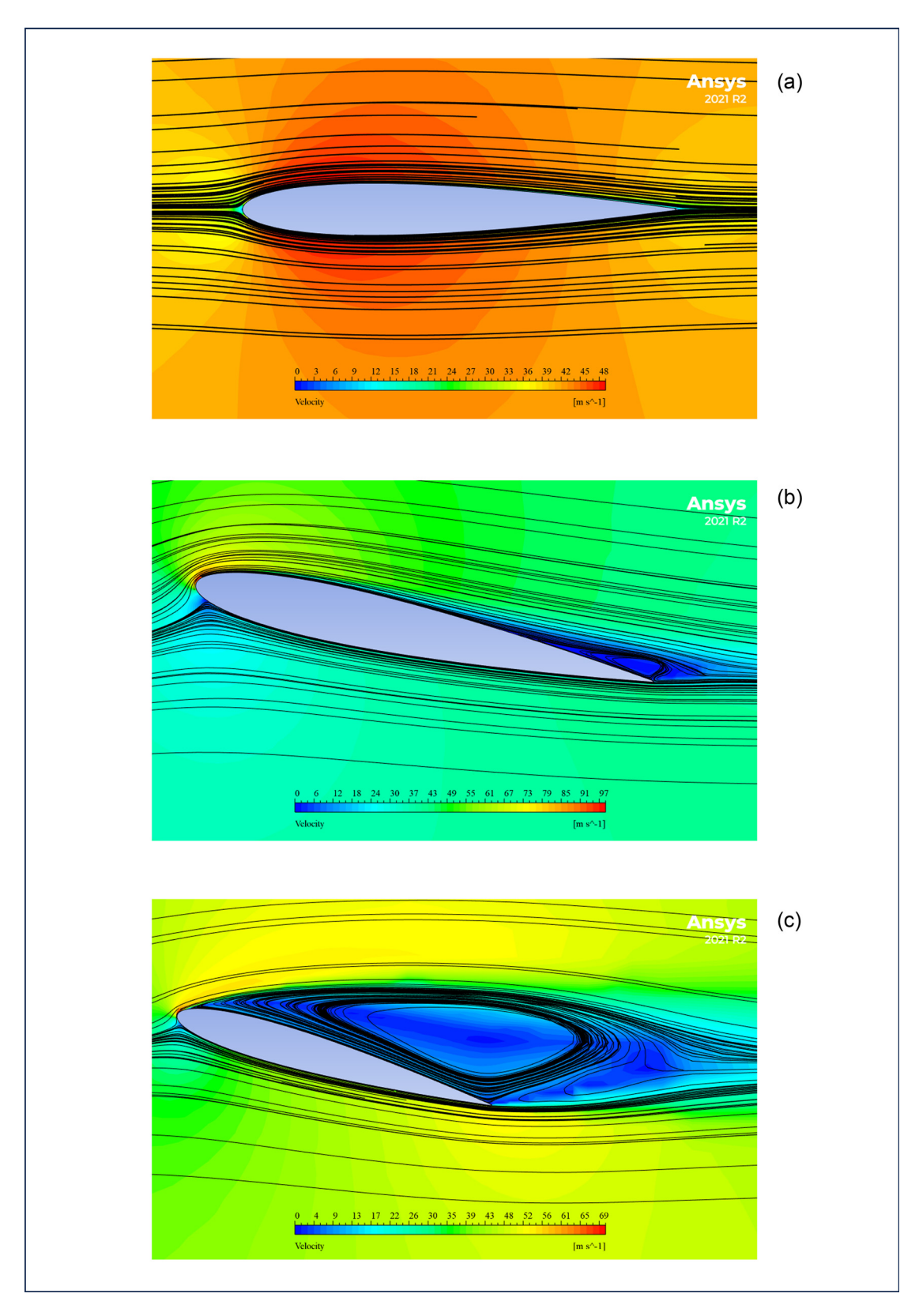


**Figure 8:** Velocity contours and streamlines of airfoil NACA0012 that Re =  $4 \times 10^5$  and at AOA: (a) =  $0^\circ$ , (b) =  $14^\circ$ , and (c) =  $18^\circ$ .

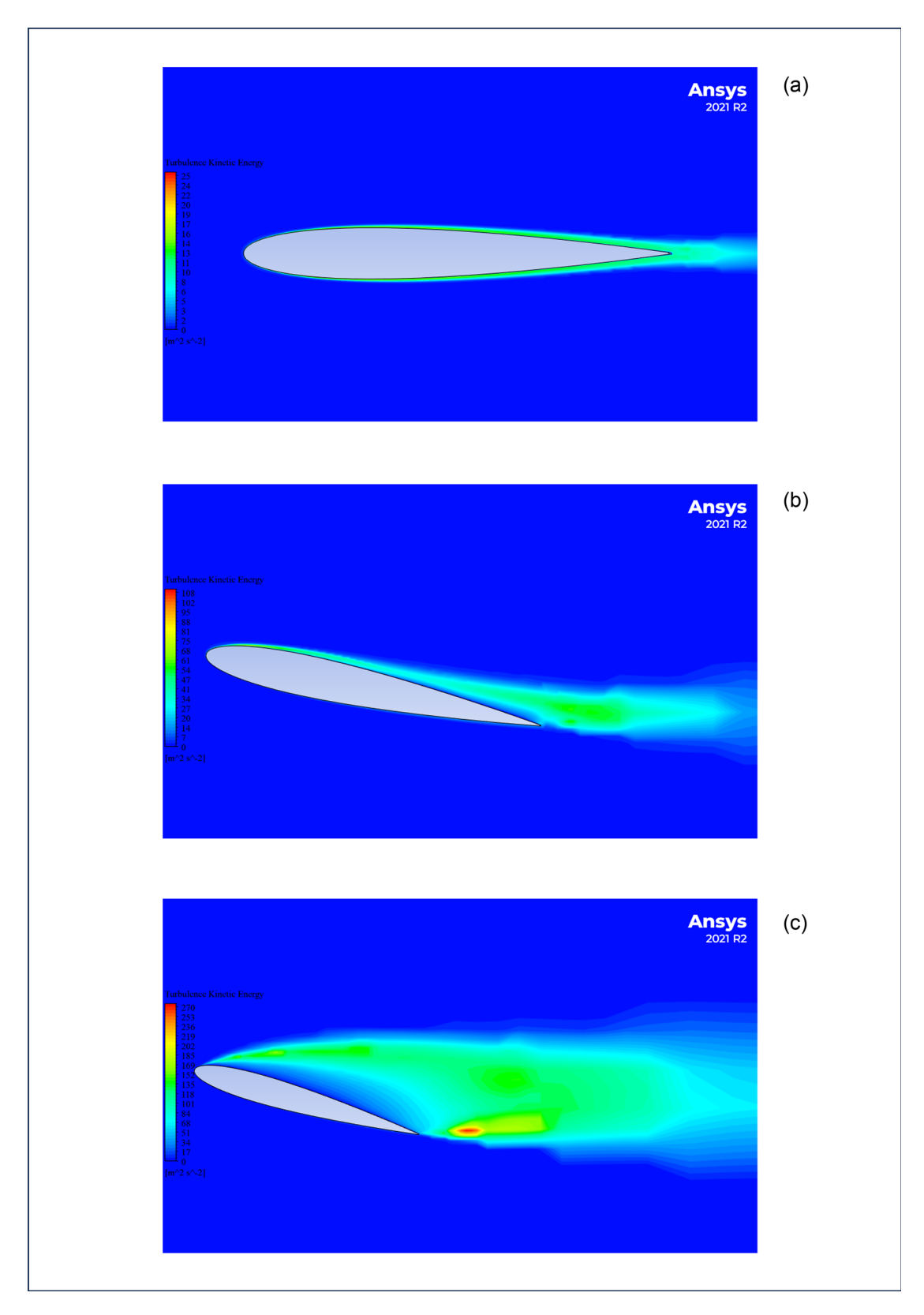


Figure 9: TKE contours of airfoil NACA0012 that Re =  $4 \times 10^5$  and at AOA: (a) =  $0^\circ$ , (b) =  $14^\circ$ , and (c) =  $18^\circ$ .

Table 4: Numerical results for various AOAs at Reynolds number

AOA	Re = 8 × 10 <sup>4</sup>			Re = 2 × 10 <sup>5</sup>		Re = 3 × 10 <sup>5</sup>			Re = 4 × 10 <sup>5</sup>			
	<b>C</b> <sub>D</sub>	C <sub>L</sub>	C <sub>L</sub> /C <sub>D</sub>	C <sub>D</sub>	C <sub>L</sub>	C <sub>L</sub> /C <sub>D</sub>	<b>C</b> <sub>D</sub>	C <sub>L</sub>	C <sub>L</sub> /C <sub>D</sub>	C <sub>D</sub>	C <sub>L</sub>	$C_L/C_D$
0°	0.024	0.004	0.162	0.020	0.010	0.503	0.018	0.014	0.775	0.017	0.013	0.792
2°	0.025	0.108	4.363	0.020	0.118	5.871	0.018	0.123	6.674	0.017	0.131	7.882
4°	0.025	0.212	8.422	0.021	0.227	11.054	0.018	0.232	12.600	0.017	0.236	13.735
6°	0.028	0.425	15.097	0.023	0.458	19.921	0.021	0.470	22.670	0.019	0.476	24.558
8°	0.033	0.603	18.438	0.026	0.640	24.271	0.024	0.655	27.491	0.022	0.666	29.847
10°	0.041	0.783	18.929	0.033	0.840	25.458	0.030	0.873	29.043	0.028	0.891	31.552
12°	0.056	0.896	16.143	0.043	0.979	22.899	0.039	1.019	26.327	0.036	1.040	28.697
14 <sup>0</sup>	0.160	0.586	3.655	0.131	0.781	5.985	0.089	0.968	10.827	0.051	1.124	21.908
16°	0.192	0.637	3.319	0.200	0.693	3.473	0.216	0.729	3.371	0.176	0.795	4.527
18°	0.260	0.717	2.754	0.245	0.702	2.860	0.237	0.702	2.966	0.233	0.726	3.113

Table 5: Experimental results for various AOAs at Reynolds number

AOA	I	Re = 8 × 1	04	Re = 2 × 10 <sup>5</sup>			
	C <sub>D</sub>	C <sub>L</sub>	C <sub>L</sub> /C <sub>D</sub>	C <sub>D</sub>	C <sub>L</sub>	$C_L/C_D$	
0°	0.023	0.004	0.512	0.019	0.010	0.161	
2°	0.024	0.105	6.045	0.019	0.116	4.401	
4°	0.024	0.199	11.070	0.020	0.216	8.220	
6°	0.027	0.417	20.851	0.021	0.445	15.514	
8°	0.031	0.590	25.556	0.025	0.627	19.086	
10°	0.037	0.735	26.829	0.030	0.799	19.869	
12°	0.050	0.882	24.142	0.040	0.965	17.605	
14°	0.135	0.543	6.514	0.113	0.735	4.016	
16°	0.188	0.593	3.868	0.167	0.645	3.150	
18°	0.230	0.644	2.972	0.221	0.657	2.800	

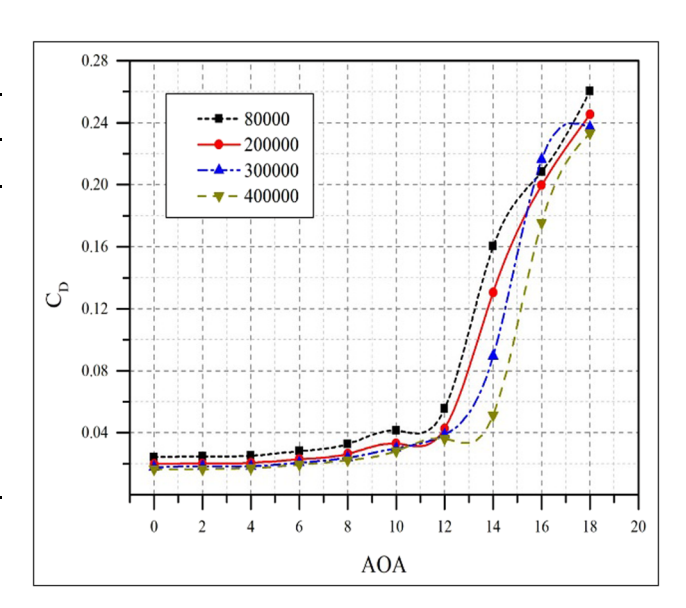
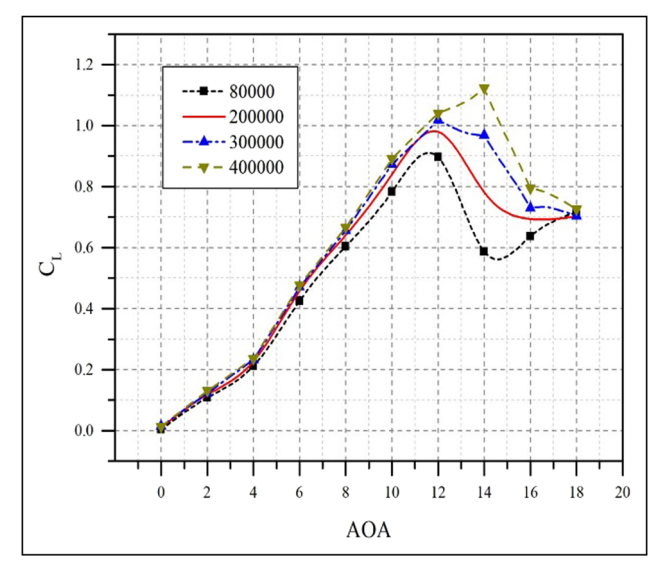
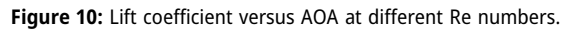
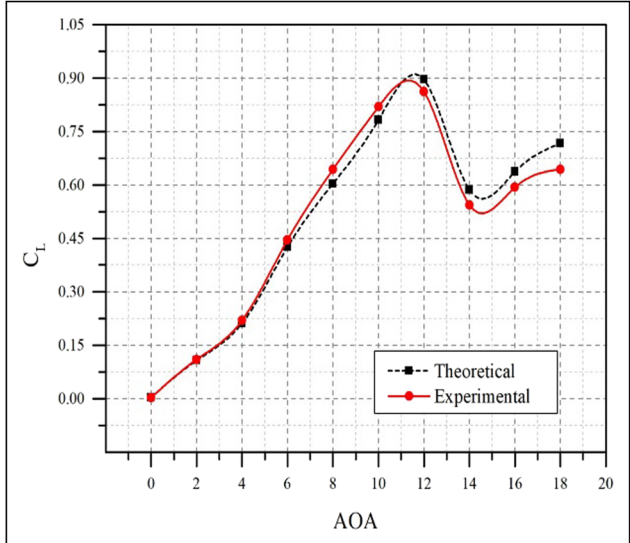


Figure 11: Drag coefficient against AOA at different Re numbers.







**Figure 12:** Lift coefficient comparison with AOA at Re =  $8 \times 10^4$ .

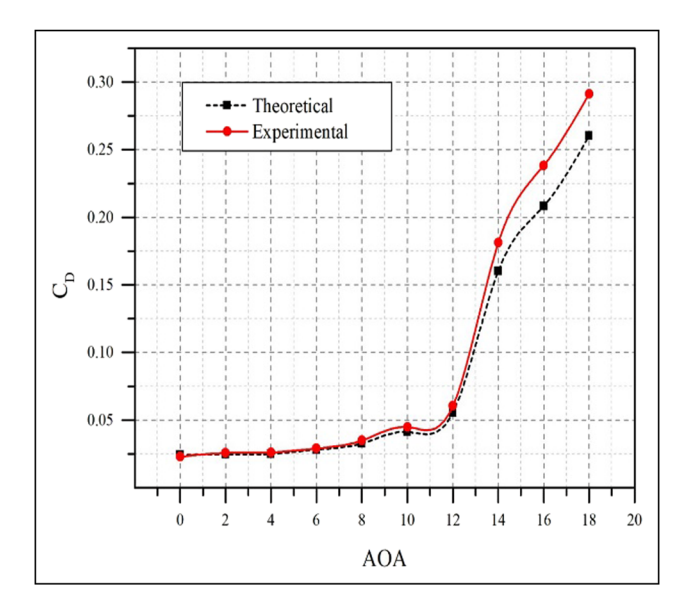
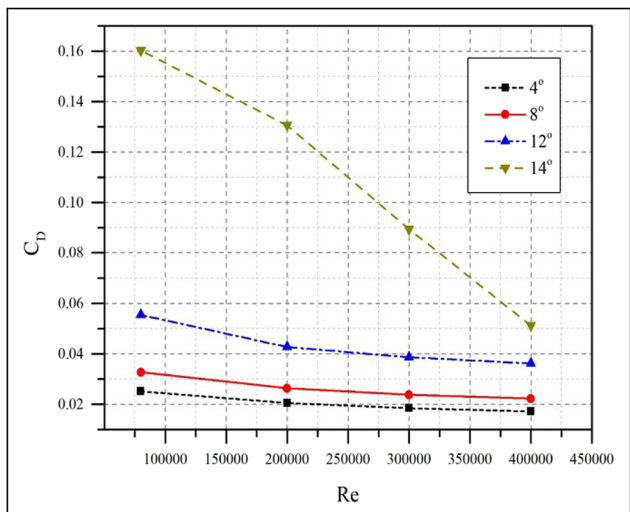


Figure 13: Drag coefficient comparison with AOA at Re =  $8 \times 10^4$ .



**Figure 15:** Effect of Re number on the drag coefficient at AOAs of  $4^{\circ}$ ,  $8^{\circ}$ ,  $12^{\circ}$ , and  $14^{\circ}$ .

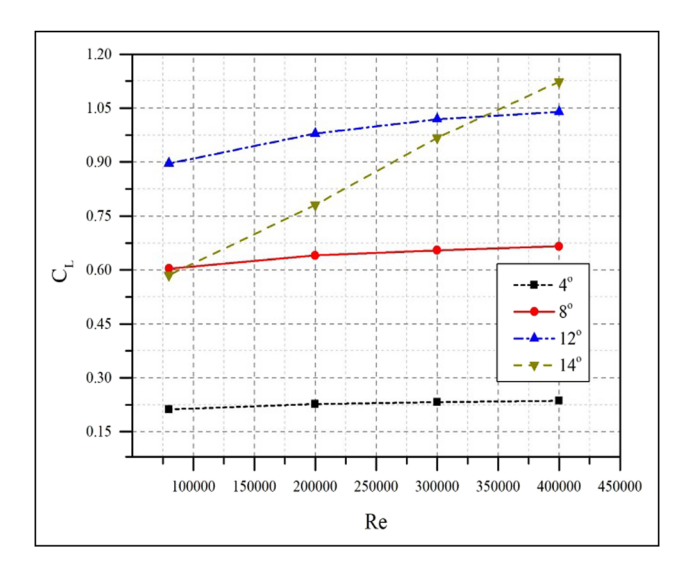
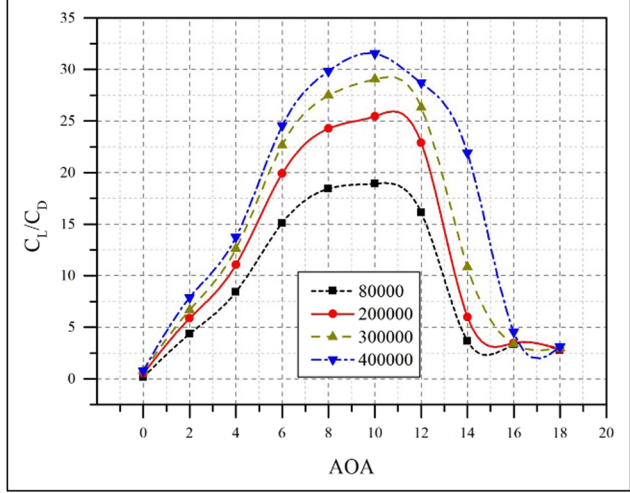


Figure 14: Effect of Re number on the lift coefficient at AOAs of  $4^{\circ}$ ,  $8^{\circ}$ ,  $12^{\circ}$ , and  $14^{\circ}$ .

the experimental and numerical results. The stall angle is similar in the experimental and numerical studies and is  $12^\circ$  with an error of 2% for  $C_{\rm L}$  and an error of 7% for  $C_{\rm D}$ . After reaching the stall angle, the curves start to decrease in both experimental and numerical studies. As the AOA increases, the error becomes prominent, reaching the highest value of 10% for  $C_{\rm L}$  and 16% for  $C_{\rm D}$ . These values correspond to the high velocity of separation of the adjacent layer, further leading to the formation of vortices on the upper surface of the airfoil. The same behavior can be observed at Re =  $2\times10^5$ , with the only difference being the lower error value between the experimental and numerical modeling results.



**Figure 16:**  $C_L/C_D$  against AOA at different Re numbers.

#### 6.3 Effect of Re on $C_{\rm L}$ and $C_{\rm D}$

The Re number, a nondimensional number with great importance in fluid mechanics applications, is defined as the ratio of the inertial force to the viscous force. Thus, the Re number can help to determine the relative importance of these forces under certain flow conditions. The effect of Re on the stall angle and the lift and drag coefficients is illustrated in Figures 14 and 15. In Figure 15, the lift coefficient reaches its maximum of 0.896, 0.979, and 1.0188 at the stall angle of 12° and Re numbers of 8 × 10<sup>4</sup>, 2 × 10<sup>5</sup>, and 3 × 10<sup>5</sup>; it also reaches the maximum at 1.1235 at the stall angle of 14° at Re = 4 × 10<sup>5</sup>, which can be attributed to

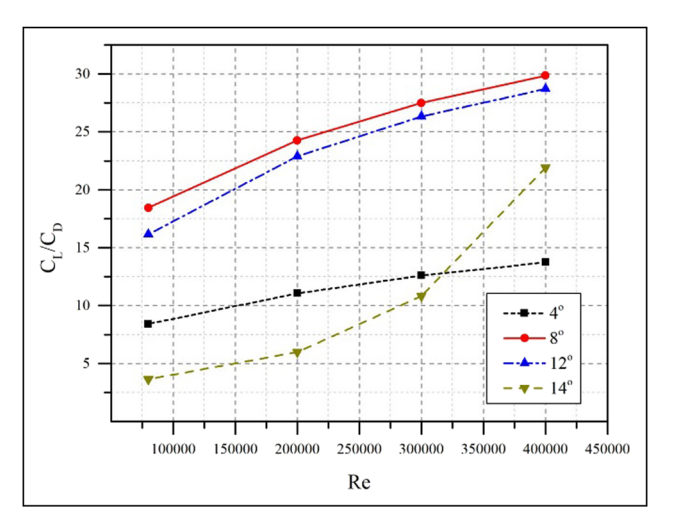


**Figure 17:**  $C_{\rm L}/C_{\rm D}$  against Re value at AOAs of 10° and 12°.

the delayed flow separation on the airfoil surface with increasing AOA and Re. The increasing Re directly affects the size of the vortex from which the flow separation originates. The drag coefficient reaches its maximum of 1.1235 at an AOA of  $14^{\circ}$  and Re =  $8 \times 10^{4}$ ,  $2 \times 10^{5}$ ,  $3 \times 10^{5}$ , and  $4 \times 10^{5}$ . The findings indicate that changing the Re number in small increments has a negligible effect on the aerodynamic properties of airfoils because it entails only slight changes in the locations of the perturbed laminar transition.

#### 6.4 Effect of AOA and Re on $C_{\rm L}/C_{\rm D}$

Simply relying on aircraft design is insufficient in generating lift, as a high  $C_{\rm L}/C_{\rm D}$  ratio must be gained to increase the flying distance of aircraft, especially when heavy weights are involved. The  $C_{\rm L}/C_{\rm D}$  ratio, generally regarded as the efficiency of the airfoil, is the ratio between the lift resulting from the airfoil to the drag resulting from its movement in air. The  $C_{\rm L}/C_{\rm D}$  ratio increases with increasing lift coefficient, i.e., it is directly proportional to each of the Re numbers and the AOA until the stall angle is reached. Table 4 shows the values of  $C_{\rm L}/C_{\rm D}$  for AOAs ranging from 0° to 18° at different Re numbers. Figures 16 and 17 show the graphs of  $C_{\rm L}/C_{\rm D}$  with varying low Re numbers and AOAs, respectively. As the AOA continuously increases and flow separation occurs, the  $C_{\rm L}/C_{\rm D}$  ratio decreases due to the sudden decrease in the lift coefficient and the rapid increase in the drag coefficient.

#### 7 Conclusion

In the current research, experimental and numerical study was conducted for the symmetrical NACA 0012 airfoil at

various AOAs and low Re numbers. The computational analysis was carried out on the ANSYS FLUENT R2 platform using the  $k-\omega$  SST turbulence model, while the experimental investigation was carried out in a wind tunnel device with dimensions of  $305 \times 305 \times 600$  mm. The results of this study may be summed up as follows:

- The NACA 0012 airfoil has a non-cambered airfoil shape, which prevents lift at an AOA equal to 0°. Also, between airfoil surfaces, there is no difference in pressure.
- The lift coefficient rises linearly with the AOA increased until it reaches its maximum value ( $C_L$  max) at a certain angle known as the stall angle. However, as the AOA increases further, the flow encounters high opposite-pressure gradients it is hard to beat, leading to flow separation and the formation of eddies. This causes the airfoil to experience lower flow velocity and higher turbulence intensity on its upper surface. Consequently, the pressure on the top of the airfoil increases, resulting in a continuous decrease in the lift coefficient.
- The drag coefficient on the airfoil increases with the AOA increased, where this increase leads to transitioning the flow from laminar to turbulent. As turbulence intensifies, the flow separates from the airfoil surface due to eddies created by the turbulence. This leads to a decrease in the lift coefficient and an increase in resistance, leading to poor airfoil performance.
- As the Reynolds number rises, the free current's disturbance also rises, giving the boundary layer more TKE and causing it to stay connected to the surface for a longer period compared with lower Re numbers. The lift coefficient is somewhat lower at the lesser Reynolds number at higher AOAs due to the trailing edge flow separation. Additionally, increasing the Reynolds number results in an increase in the stall angle (C<sub>L</sub> max).
- Based on the aforementioned findings, additional thorough investigation into the AOA or investigating the connection between asymmetric airfoils and the current study is required, clarifying their applicability. Enhancing airfoil performance with the inclusion of lifting devices, such as flaps and slats, is another area that merits investigation. Researchers in the discipline may want to consider these suggestions as potential future study topics.

**Acknowledgements:** The authors express gratitude to the Department of Aeronautical Engineering, Technical Al-Furat Al-Awsat Technical University (ATU)/Republic of Iraq, for providing wind tunnel and technical support that enabled successful study completion and the achievement of desired results. They express gratitude for their cooperation and distinction.

**Conflict of interests:** The authors declare that they have no conflict of interest.

**Data availability statement:** Most datasets generated and analyzed in this study are comprised in this submitted manuscript. The other datasets are available on reasonable request from the corresponding author with the attachedinformation.

#### References

- [1] Sadikin A, Yunus NAM, Abd Hamid SA, Salleh SM, Rahman MNA, Mahzan S, et al. A comparative study of turbulence models on aerodynamics characteristics of a NACA0012 airfoil. Int J Integr Eng. Apr. 2018;10(1):134–7.
- [2] Shabur M, Khan AH, Rayhan S. Turbulent kinetic energy analysis of NACA0012 and NACA0018 airfoils at two reynolds number using CFD tool. Sci Open Prepr. 2022;0–16.
- [3] Martínez-Aranda S, García-González AL, Parras L, Velázquez-Navarro JF, Del Pino C. Comparison of the aerodynamic characteristics of the NACA0012 airfoil at low-to-moderate Reynolds numbers for any aspect ratio. Int J Aerosp Sci. 2016;4(1):1–8.
- [4] Singh M. Fabrication and Analysis of NACA 0012 Airfoil in Wind Tunnel. Int Res J Eng Technol. May 2018;5(no. 5):4150–8.
- [5] Kunjumon AP, Koshy FM, Jacob ST. Determination of Pressure Coefficient Around Naca Airfoil. Int J Appl Eng Res. 2019;14(14):81–7.
- [6] Raval NP, Malay M, Jitesh L. CFD analysis of NACA0012 aerofoil and evaluation of stall condition. Int J Eng Technol Sci Res. Apr. 2017;4(4):57–60.
- [7] Patel A, Thakor R. Numerical analysis of NACA0012 using CFD. Int J Anal Exp Modal Anal. Jun. 2020;XII(VI):1244–53.

- [8] Mallela G, Paturu P, Komaleswarao M. Lift and drag performance of NACA0012 airfoil at various angle of attack using CFD. Int J Mech Prod Eng Res Dev. 2018;8(3):89–100. doi:10.24247/ijmperdjun201810.
- [9] Yuta Y, Tomohisa O, Akinori M. Pressure distributions on NACA0012 AIRFOIL at low reynolds numbers. In 2013 The Proceedings of the International Conference on Jets Wakes and Separated Flows (ICJWSF).
- [10] Kabir A, Hasan M, Akib YM. Numerical analysis on NACA 0012 airfoil at different Mach numbers with varying angle of attacks using computational fluid dynamics. 5th Int. Conf. Eng. Res. Innov. Educ. (ICERIE), 2019 At Shahjalal Univ. Sci. Technol. (SUST), Sylhet, Bangladesh; 2019. p. 1–6.
- [11] Shahariar GH. Numerical analysis and comparison on aerodynamics characteristics on NACA-0012 & NACA-4412. International Conf. Mech. Ind. Energy Eng, 2014; 2014. p. 2. Available: https://www.academia.edu/10488400/Numerical\_Analysis\_and\_Comparison\_on\_Aerodynamics\_Characteristics\_on\_NACA-0012\_and\_NACA-4412.
- [12] Sahoo S, Maity S. CFD analysis of responses of two-equation turbulence models for flow over NACA 0012, NACA 4412 and S809 aerofoils. In Advances in Mechanical Engineering: Select Proceedings of ICRIDME. Singapore: Springer; Jan. 2020. p. 31–40.
- [13] Jha S, Gautam U, Narayanan S, Dhas LK. Effect of reynolds number on the aerodynamic performance of naca0012 aerofoil. In IOP Conference Series: Materials Science and Engineering. Sikkim, India: IOP Publishing, vol. 377, Issue 1; December 2017. p. 1–10.
- [14] Yousefi K, Razeghi A. Determination of the critical Reynolds number for flow over symmetric NACA airfoils. In 2018 AIAA Aerospace Sciences Meeting; Jan 2018. p. 1–11.
- [15] Eftekhari S, Al-Obaidi ASM. Investigation of a NACA0012 finite wing aerodynamics at low Reynold's numbers and 0° to 90° angle of attack. J Aerosp Technol Manag. 2019;11:1–11. doi: 10.5028/jatm. v11.1023.
- [16] Çengel YA, Cimbala JM. Fluid mechanics: fundamentals and applications. Mc-Graw-Hill; 2006.
- [17] Prasad KS, Krishna V, Kumar BBA. Aerofoil profile analysis and design optimisation. J Aerosp Eng Technol. 2013;3(2):1–10, Available: https://www.researchgate.net/publication/279186627.